Conference on Modelling Fluid Flow (CMFF'25)
The 19th International Conference on Fluid Flow Technologies
Budapest, Hungary, August 26 - August 29, 2025

STUDY OF THE MIXING PERFORMANCE OF CURVED BLADE TURBINES IN A SOLID-LIQUID DUAL IMPELLER STIRRED SYSTEM

Laifa Lu[1,2], Jiacheng He[1,2], Shuiqing Zhou[1,2], Weiya Jin[1,2], Zengliang Gao[1,2], Diping Xu[1,2]

[1] College of Mechanical Engineering, Zhejiang University of Technology, Hangzhou,310023, China.
[2] Institue of Innovation Research of Shengzhou and Zhejiang University ofTechnology, Shengzhou,312400, China.
[3] Corresponding Author. College of Mechanical Engineering, Zhejiang University of Technology, Hangzhou 310023, China. E-mail: zsqwh666@163.com

ABSTRACT

Improving mixing efficiency, product quality and process sustainability are the core challenges in the design of multi-impeller stirred tank reactors. In this study, Euler-Euler numerical simulation and Particle Image Velocimetry (PIV) technology were used to systematically explore the solid-liquid mixing performance in a double-impeller mixing tank. Combined with the surrogate model and sensitivity analysis method, the flow field characteristics and suspension performance in the mixing tank of itched blade turbine (PBT) and curved blade turbine (CBT) were studied qualitatively and quantitatively. The results show that the solid-liquid suspension performance of CBT is better than that of PBT. The arc chord distance of the upper impeller and the blade angle have a great influence on the power consumption and particle distribution. When the arc chord distance of the upper impeller is 4mm and the blade inclination angle is 50°, the stirred tank can significantly improve the mixing performance and reduce the power consumption. The research results have certain guiding significance for the optimization design of curved blade turbine and similar mixing tank.

Keywords: solid-liquid mixing, CFD, PIV, sensitivity analysis

NOMENCLATURE

B	[mm]	baffle width
C	[mm]	off-bottom clearance
D	[mm]	impeller diameter
d_s	[mm]	solid particles diameter
g	[m/s^2]	gravitational acceleration
H	[mm]	liquid height
h	[mm]	baffle height
K	[-]	interphase momentum transfer coefficient
p	[Pa]	phase pressure
S	[mm]	blade spacing
T	[mm]	tank diameter
α	[-]	phase volume fraction
θ	[K]	particles temperature
λ	[m^2/s]	phase dynamic viscosity
μ	[$Ps{\cdot}s$]	phase dynamic viscosity
ρ	[kg/m^3]	phase density
τ	[-]	viscous stress tensor of phase

Subscripts and Superscripts

l	liquid phase
s	solid phase
u	upper impeller

1. INTRODUCTION

As a typical fluid machinery, the multi-impeller stirred tank has been widely used in the industrial field due to its excellent mixing and mass transfer performance [1]. However, with the development of the industry, the requirements for hydraulic performance, mixing efficiency and energy consumption are increasing [2], and the mixing equipment is facing the trend of transformation and upgrading. The traditional empirical standard design method is difficult to meet the growing demand for product performance. It has become a hot issue for scholars at home and abroad to improve the comprehensive performance of the tank by designing a new stirring main structure [3].

The solid-liquid double impeller stirred tank is one of the conventional multi-impeller reaction equipment, and its solid particle suspension performance directly affects the product crystallization and precipitation quality [4, 5]. In order to optimize the performance of the mixing tank, the process parameters are often used as the research object. Gu et al. [6] found that at the same speed, the

fractal blade impeller is superior to the inclined blade impeller in terms of particle dispersion. Davoody et al. [7] showed that the impeller parameters were the key factors affecting the performance of the mixing system, and the structure of the curved blade impeller had a significant effect on the volumetric mass transfer coefficient of the gas-solid-liquid three-phase mixing. The above research shows that the non-standard blade structure design at the appropriate scale can effectively improve the mixing efficiency.

Nowadays, Computational Fluid Dynamics (CFD) has been widely used in the performance analysis of various types of stirred tanks, which can effectively simulate the nonlinear and strong pulsation characteristics in the flow field [8]. However, numerical simulation methods usually need to be combined with experimental analysis to verify the accuracy of the prediction results. Martina et al. [9] used conductance probe to measure the local solid concentration at different heights and radial positions in the container, and studied the particle distribution and suspension state. Guha et al. [10] used radioactive particle tracer technique to investigate the hydrodynamic characteristics of high concentration solid-liquid suspension system in stirred tank, which provided data support for evaluating the accuracy of CFD model of slurry reactor. Montante et al. [11] used Particle Image Velocimetry (PIV) technology to study the behavior of dilute solid particles, and analyzed the influence of dispersed phase on the average velocity and turbulence intensity of continuous phase. The purpose of this study is to combine CFD and PIV methods to optimize the performance of mixing tanks more conveniently and accurately.

In order to clarify the optimization direction in the design process, many scholars have introduced sensitivity analysis technology to identify the key parameters that affect the design objectives [12, 13]. In this study, the effects of key structural parameters of the curved blade turbine on the solid-liquid mixing performance were systematically analyzed by Euler-Euler numerical calculation and PIV experimental technology, combined with Multiple-response Gaussian Process (MRGP) approximation model and Extended Fourier Amplitude Sensitivity Testing (EFAST) method. Finally, a curved blade turbine structure with better comprehensive performance was obtained, and the optimization results were verified by PIV test.

2. CALCULATION METHOD AND MODEL VALIDATION

2.1. Numerical simulation calculation method

In this study, the Eulerian-Eulerian multiphase flow model is used to simulate the flow of two phases, each of which is considered as a mutually coherent continuum, in order to solve the Reynolds-averaged continuity equation and the momentum conservation equation for each phase. The controlling equations for phase q (liquid phase q=l, solid phase q=s) are as shown below [14]:

Continuity equation:

$$\frac{\partial}{\partial t}\left(\alpha_{\mathrm{q}}\rho_{\mathrm{q}}\right)+\nabla\bullet\left(\alpha_{\mathrm{q}}\rho_{\mathrm{q}}\vec{u}_{\mathrm{q}}\right)=0 \tag{1}$$

where α_{q} is the volume fraction of the q-phase, $\vec{u}_{\mathrm{q}}$ is the velocity of the q-phase, and ρ is the density of the q-phase.

Liquid phase momentum conservation equation:

$$\begin{aligned}&\frac{\partial}{\partial t}\left(\alpha_{\mathrm{l}}\rho_{\mathrm{l}}\vec{u}_{\mathrm{l}}\right)+\nabla\bullet\left(\alpha_{\mathrm{l}}\rho_{\mathrm{l}}\vec{u}_{\mathrm{l}}\vec{u}_{\mathrm{l}}\right)=\\&-\alpha_{\mathrm{l}}\nabla p+\nabla\bullet\bar{\bar{\tau}}_{\mathrm{l}}+K\left(\vec{u}_{\mathrm{l}}-\vec{u}_{\mathrm{s}}\right)+\alpha_{\mathrm{l}}\rho_{\mathrm{l}}\vec{g}\end{aligned} \tag{2}$$

where p denotes the thermodynamic pressure, $\vec{g}$ is the gravitational acceleration, $\bar{\bar{\tau}}$ is the viscous stress tensor of the liquid phase, and K is the interphase momentum transfer coefficient.

Solid phase momentum conservation equation:

$$\begin{aligned}&\frac{\partial}{\partial t}\left(\alpha_{\mathrm{s}}\rho_{\mathrm{s}}\vec{u}_{\mathrm{s}}\right)+\nabla\bullet\left(\alpha_{\mathrm{s}}\rho_{\mathrm{s}}\vec{u}_{\mathrm{s}}\vec{u}_{\mathrm{s}}\right)=\\&-\alpha_{\mathrm{s}}\nabla p-\nabla p_{\mathrm{s}}+\nabla\bullet\bar{\bar{\tau}}_{\mathrm{s}}+K\left(\vec{u}_{\mathrm{l}}-\vec{u}_{\mathrm{s}}\right)+\alpha_{\mathrm{s}}\rho_{\mathrm{s}}\vec{g}\end{aligned} \tag{3}$$

where $\bar{\bar{\tau}}$ is the viscous stress tensor of the solid phase, and p_s is the solid phase pressure.

In this study, a *k*-*ε* mixed turbulence model is used to calculate the turbulent kinetic energy and dissipation rate of the liquid phase, assuming that both phases have the same *k* and *ε*. The *k* and *ε* equations describing the model are as follows:

$$\begin{aligned}&\frac{\partial}{\partial t}\left(\rho_m k\right)+\nabla\cdot\left(\rho_m\vec{u}_m k\right)=\\&\nabla\cdot\left(\mu_m+\frac{\mu_{\mathrm{t,m}}}{\sigma_{\mathrm{k}}}\nabla k+G_{\mathrm{k,m}}+G_{\mathrm{b,m}}-\rho_m\varepsilon\right)\end{aligned} \tag{4}$$

$$\begin{aligned}&\frac{\partial}{\partial t}\left(\rho_m\varepsilon\right)+\nabla\cdot\left(\rho_{\mathrm{m}}\vec{u}_{\mathrm{m}}\varepsilon\right)=\\&\nabla\cdot\left(\frac{\mu_{\mathrm{t,m}}}{\sigma_\varepsilon}\nabla\varepsilon\right)+\frac{\varepsilon}{k}\left(C_{1\varepsilon}G_{\mathrm{k,m}}-C_{2\varepsilon}\rho_m\varepsilon\right)\end{aligned} \tag{5}$$

where ρ_m is the mixture density, μ_m is the molecular viscosity, $\vec{u}_m$ is the velocity.

Neglecting the effects of virtual mass force, lift force and mass transfer, this paper only considers the drag force which has a large impact on the simulation

results [15]. The momentum exchange coefficients are calculated using the Huilin-Gidaspow model.

This study employs the Multiple Reference Frame (MRF) method, designating the rotating region of the impeller as the moving zone and the remaining regions as stationary zones. A pressure-based transient implicit solver was utilized, with pressure-velocity coupling handled by the Phase Coupled SIMPLE algorithm. A second-order upwind differencing scheme was adopted, with the convergence criterion set to variable residuals falling below 10^{-4} or exhibiting stabilized residual curves. Standard wall functions were applied to model near-wall fluid motion. The top boundary was assigned a symmetric boundary condition to simulate the free surface, while all other geometric walls were assumed to have no-slip boundary conditions.

2.2. PIV Experimental validation

With the development of experimental measurement techniques, PIV is widely used in hydrodynamic measurements as a non-contact type measurement technique capable of providing rich fluid flow information for stirred reactors. In this study, a 2D PIV system was used. The two-dimensional (2D) PIV system adopted in the present work consisted of a dual Vlite series 532 nm dual pulse laser, a high-resolution CCD camera with 6600*4400 pixels, a synchronizer, and the commercial software MicroVec-V3.6.9 The test principle is shown in figure 1(a) and the experimental setup is shown in figure 1(b).

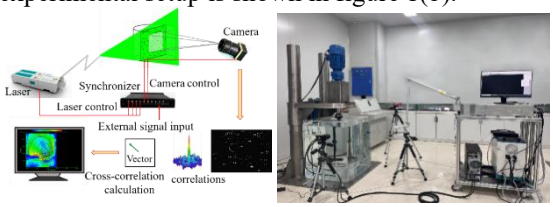

Figure 1. PIV test system (a) PIV test principle (b) PIV Experimental Apparatus

The designated region for PIV experimentation is delineated in Figure 2, wherein H signifies the cylinder's height, T corresponds to the cylinder's diameter, and B denotes the width of the baffle. The laser plane intersects the baffle plane at a 5° angle, and the LED light source forms a 30° angle with the measurement plane. This setting ensures that the image is clear and undistorted. In the context of the solid-liquid biphasic flow field under examination through PIV, the application of specific filters facilitates distinct analyses: a laser light source enables liquid flow assessment, while an LED light source enables particle flow evaluation. The PIV experiment employs fluorescent particles as tracer agents and hollow glass beads as representative solid particles. The liquid medium utilized is pure water. Table 1 provides the relevant parameters for liquid and solid particles.

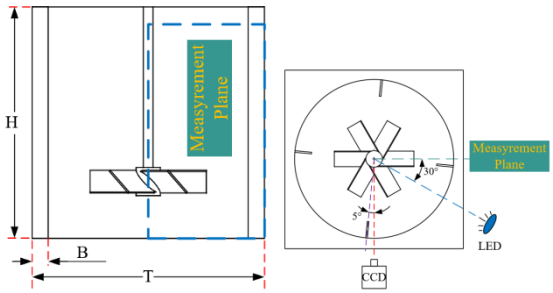

Figure 2. PIV measurement area (a) Mixing tank (b) PIV measurement plane

Table 1. Physical properties parameters

Parameter	Symbol	Value
Liquid density	ρ_L	1000kg/m^3
Hydrodynamic viscosity	μ	0.001Pa·s
Solid particles density	ρ_S	1430 kg/m^3
Solid particles diameter	d_S	0.15mm
Solid volume fraction	φ_S	5.6%

Owing to the inherent rotational periodicity of the stirring process, only half the flow area requires measurement during flow field characterization in stirred tanks. As depicted in Figure 3, liquid-phase average velocity fields obtained from numerical simulations and PIV experiments demonstrate close agreement. Within the r/R range of 0.3 to 0.4, a circulating vortex structure forms near the blade tip, from which fluid discharges diagonally downward at maximum velocity. Upon impinging the tank bottom, the majority of fluid establishes impeller-induced global circulation, while localized particles gradually settle to form an inverted conical region at the base.

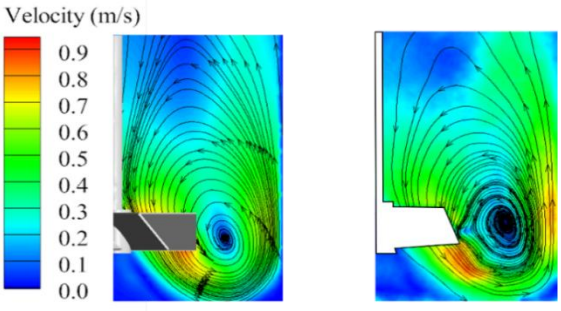

Figure 3. Fluid mean velocity field (a) CFD simulation (b) PIV experiment

3. RESEARCH OBJECT AND ITS PARAMETERIZATION

3.1. Stirring equipment

In the context of a mixing tank characterized by a substantial height-to-diameter ratio, the utility of a solitary impeller becomes limited. This study focuses on a dual-impeller configuration for solid-liquid mixing, as illustrated in Figure 4. The primary

flow field constituents encompass the tank body, tank bottom, baffle, and agitator, encompassing the mixing shaft, upper impeller, and lower impeller. Refer to Table 2 for the structural specifications of the mixing tank and impeller. Within the prototype configuration, the upper and lower impellers are designed as pitched blade turbine (PBT), representing a prevalent choice for mixed-flow impellers within solid-liquid mixing systems. Both impellers are in up pumping mode.

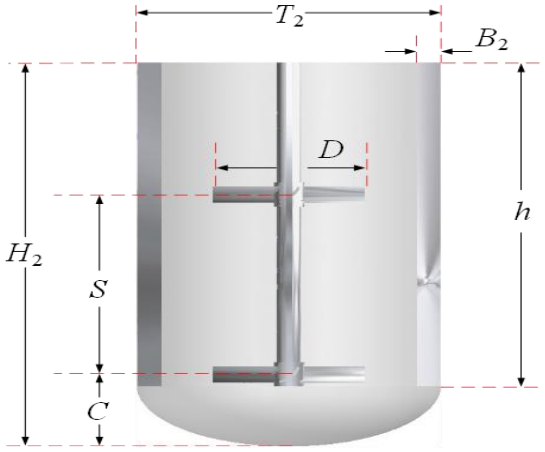

Figure 4. Structure of dual impeller mixing tank

Table 2. Structural parameters of mixing tank and impeller

Parameter	Symbol	Value
Tank diameter	T	500 mm
Liquid height	H_2	1.6 T
Baffle width	B_2	0.1 T
Baffle height	h	1.35 T
Impeller diameter	D	0.5 T
Off-bottom clearance	C	0.3 T
Blade spacing	S	0.75 T

3.2. Impeller structure parameterization

The structural characteristics of the stirrer significantly influence the tank's flow field and the mixing performance of two-phase media. Axial impellers are good for improving the deposition of particles at the bottom, while the shear flow generated by radial impellers is crucial for particle suspension. In the dual impeller mixing tank under study, impeller size, blade spacing, and off-bottom clearance all affect particle suspension performance. However, due to constraints from the shaft bore and motor positioning, the latter is typically difficult to adjust. Traditional PBT impellers fail to meet practical requirements, making impeller structural redesign essential. Consequently, a curved blade turbine (CBT) design is introduced aimed at enhancing energy utilization efficiency. Figure 5 illustrates the structural configuration of the CBT impeller.

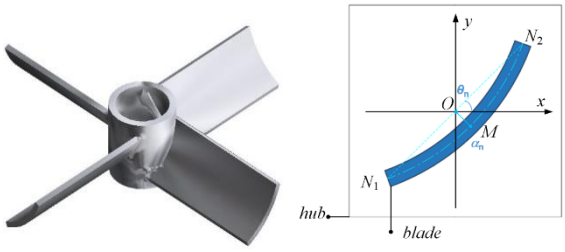

Figure 5. Impeller structure diagram (a) CBT impeller (b) structure parameters of impeller

As in Figure 5, the cross-sectional profile of the blade is shown schematically. The point O is the center of the impeller hub, and there is a straight line N_1N_2 across the point O, which is the chord length of the curved blade, and N_1MN_2 is the mid-arc of the blade. In this study, the position of point O is fixed, and the length of straight line N_1N_2 is unchanged. Take the upper impeller OM distance as 1, ON_2 and x-axis angle as θ_1. Take the lower impeller OM distance as α_2, $ON2$ and x-axis angle as θ_2. These four parameters are the main design variables. Define α_n as the arc-chord distance and θ_n as the blade angle. When $\alpha_n = 0$ mm and $\theta_n = 45°$, the CBT form is the same as PBT.

4. SENSITIVITY ANALYSIS

A distinct interface forms between the suspended solids and the clear liquid layer in the stirred tank, and the height of this interface is defined as the cloud height. Matthias indicated that cloud height reaches full suspension at 90% of the liquid height. Therefore, the cloud height can be used as an important parameter to evaluate the mixing degree. In this study, cloud height is analyzed by numerically tracking the average solids concentration isosurface, defined as the maximum axial height of this isosurface. Taking the four parameters mentioned above as input variables, cloud height and power as output values, the corresponding surrogate model is established by MRGP model, and the sensitivity analysis of variables is carried out by EFAST method.

The MRGP model is an extension of the Kriging model. The traditional Kriging model can only deal with multivariate single response output problems, while for multi-dimensional response output, multiple Kriging models need to be constructed, and this approach does not consider the coupling-related problems of response values. Therefore, the MRGP model for multivariate multi-response problems is gradually gaining attention. MRGP model unites m functions into a specific implementation of a multi-response Gaussian process [16]:

$$G(x) = f(x)^{\mathrm{T}} B + Z(x) \tag{6}$$

where the polynomial regression function $f(x)$ is the same as the Kriging model, but the regression coefficient B is an $n*m$ matrix and $Z(x)$ is also

expanded to a *1*m* row vector. The covariance of Z(x) is expressed as a covariance matrix of size *m*m*:

$$\sum^{m}=\begin{bmatrix}\sigma^2(g_1,g_2) & \cdots & \sigma^2(g_1,g_m)\\ \vdots & \ddots & \vdots\\ \sigma^2(g_m,g_1) & \cdots & \sigma^2(g_m,g_m)\end{bmatrix} \tag{7}$$

In this paper, the MRGP model is selected as the approximation function, and the approximation model is established using the sample data of 50 sets of variables with corresponding responses obtained through Optimal Latin Hypercube Design (Opt LHD) combined with numerical simulations.

Due to the limitation of parameter selection, the constructed MRGP model will have certain errors. In order to verify the accuracy of the model, it is necessary to test it by the relevant accuracy test formula before prediction solving. In this paper, a global sensitivity analysis based on the EFAST method is used. The basic idea of the EFAST method is derived from Bayes' theorem, which holds that the sensitivity of the model output results can be reflected by the variance of the model results. The sensitivity of parameter x can be expressed by the following equation:

$$Sensitivity_{\mathrm{x}}=\frac{var_{\mathrm{x}}\left[E\left(Y|X\right)\right]}{var\left(Y\right)} \tag{8}$$

where *Y* is the output value of the model, *x* is the input parameter, *E*(*Y*|*X*) is the expectation of *Y* when *x* takes a certain value, and var_x is the variance when *x* traverses a range of values.

The total variance of the model and the first-order variance due to parameter *i*, neglecting the coupling with other parameters, yields the first-order sensitivity values:

$$S_{\mathrm{i}}=\frac{\mathrm{var}_{\mathrm{xi}}\left[E\left(Y|x_{\mathrm{i}}\right)\right]}{var(Y)} \tag{9}$$

And for the total sensitivity index of a parameter i after considering the effect of parameter coupling, we need to consider the coupling part between the parameters:

$$S_{\mathrm{Ti}}=1-\frac{var_{\mathrm{xi}}\left[E\left(Y|x_{\mathrm{-i}}\right)\right]}{var(Y)} \tag{10}$$

The first-order sensitivity indicates the degree of influence of a single influencing factor on cloud height and power, while the overall sensitivity reflects not only the degree of influence of a single influencing factor on cloud height and power, but also the interaction with other influencing factors. Therefore, when the difference between the first-order sensitivity of a variable and the overall sensitivity is large, it can be considered that the factor has an obvious interaction. The normalized influence factors of each variable parameter are shown in Figure 6.

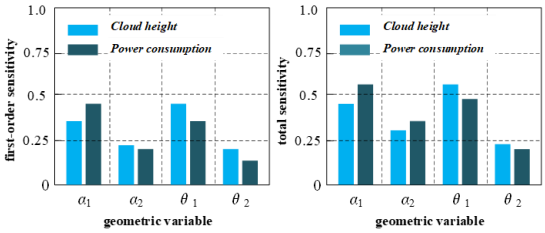

Figure 6. Influence factors of different variables (a) First-order sensitivity (b) Total sensitivity

The first-order sensitivity and overall sensitivity analyses show that the upper impeller structure parameters α_1 and θ_1 have a greater degree of influence on the cloud height and power of the mixing tank. Therefore, it can be inferred that the upper impeller possesses a more significant effect on the mixing performance of the flow field. In order to reduce the complexity of the study, the subsequent study in this paper will keep the lower impeller as the prototype structure and mainly study the flow field characteristics and mixing effect of the upper impeller after the modification.

5. ANALYSIS OF RESULTS

5.1. The effect of impeller form on the flow field

Due to the symmetry of the stirring structure, the flow field shows a symmetrical distribution, which is consistent with the uniform segmentation of the baffle. Figure 7 shows the velocity contours of PBT and CBT impellers, showing similar radial and circumferential flow patterns. When the fluid rotates with the impeller, the flow in the front of the baffle is relatively smooth, but the backflow vortex will be formed after flowing through the rear of the baffle. Compared with the PBT impeller, the vortex scale generated by CBT is smaller, indicating that the mixing efficiency is higher and the energy consumption is lower. The CBT impeller design enhances the circumferential emission capacity, which can promote high-speed circulation and reduce the flow stagnation area compared to the PBT impeller.

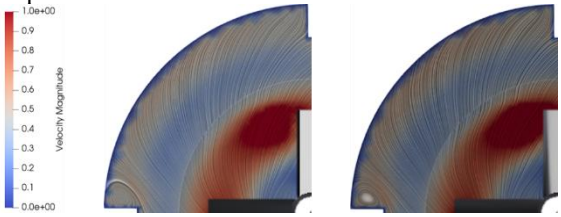

Figure 7. Plane velocity distribution of different impellers (y=0.25H₂) (a) PBT (b) CBT

It is very important to analyze the vortex structure of the impeller to optimize the efficiency of the stirred tank. Figure 8 shows the three-dimensional structure of the wake vortex downstream of the impeller blade. It can be found that each blade channel produces obvious vortex structure. These vortices absorb most of the energy transmitted by the impeller and limit its diffusion to the distant flow field. The wake vortex of PBT impeller has large scale, narrow shape and wide diffusion range, which hinders efficient energy transfer. In contrast, the CBT impeller design changes the dynamic characteristics of the wake vortex, resulting in a more compact wake and significantly reducing energy dissipation.

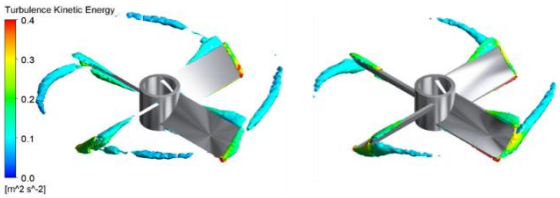

Figure 8. Three-dimensional structure of the tail vortex for different impellers (a) PBT (b) CBT

5.2. Effect of impeller form on solid phase distribution.

Understanding the distribution characteristics of solid particles within stirred tanks holds fundamental research significance. Figure 9 illustrates the three-dimensional distribution of solid-phase volume fraction. For both impeller types, particle accumulation zones form beneath the impellers while clear liquid layers emerge at the upper liquid surface. However, compared to PBT impeller, CBT impeller significantly mitigate particle sedimentation at the tank bottom while simultaneously enhancing particle suspension capability in upper regions. This demonstrates the superior mixing performance of the CBT design, attributable to its curved-blade configuration. The blade curvature expands the discharge area, generating a more powerful high-speed jet. This jet flow enhances the velocity gradient between fluid layers, increasing local energy dissipation rates and thereby improving mixing efficiency.

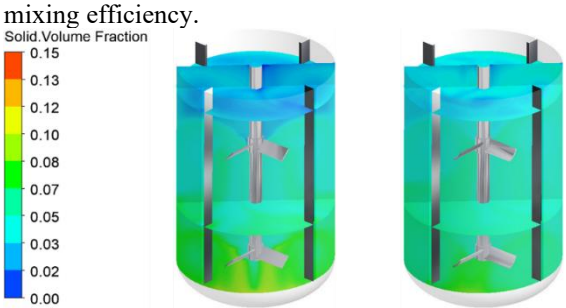

Figure 9. Overall solid phase distribution of different impellers (a) PBT (b) CBT

Figure 10 presents the solid concentration distribution along the axial height at different radial positions (r=0.1~0.9R) in the stirred tank. Compared with PBT impeller, the CBT structure shows a more uniform solid phase concentration distribution, and its concentration gradient is significantly reduced, indicating that the particle suspension performance is improved, especially in the near-axis area and near the tank wall. Under the synergistic effect of CBT and PBT double impellers, the original symmetrical flow field structure is broken, and the energy transfer efficiency between fluids is enhanced, thereby improving the mixing efficiency of the system.

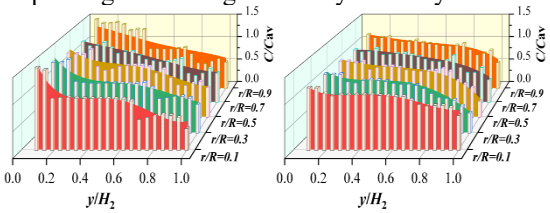

Figure 10. Local axial solid phase distribution of different impellers (a) PBT (b) CBT

5.3. The effect of arc-chord distance

Turbulent kinetic energy and turbulent energy dissipation rate serve as pivotal determinants in the assessment of both mixing duration and the quality of solid-liquid suspension [17]. Manipulation of parameters such as mixing time is facilitated by elevating turbulent kinetic energy and turbulent energy dissipation rate. The non-dimensional distribution of turbulent kinetic energy and turbulent energy dissipation rate across varying arc-chord distances is illustrated in Figures 11 and 12, respectively. Across all instances, the apex values of turbulent kinetic energy and turbulent energy dissipation rate emerge proximate to the impeller blade's tip, while values away from the blade's influence tend to be subdued. CBT engenders a discernible enhancement in the turbulent kinetic energy and turbulent energy dissipation rate within the mixing tank, particularly in proximity to the impeller. This phenomenon can be attributed to the alteration in flow field angle of incidence brought about by CBT's arc curvature. This modification augments shear forces and concurrently diminishes discharge resistance. As the arc-chord distance increases, turbulent kinetic energy and turbulent energy dissipation rate initially rise, exhibiting a slight decline once the arc-chord distance surpasses an optimal range. The most substantial increments in turbulent kinetic energy and turbulent energy dissipation rate occur at the arc-chord distance of 4 mm.

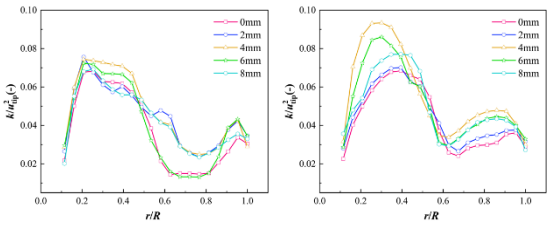

Figure 11. Effect of arc-chord distance on local radial turbulent kinetic energy (a) y = 0.25H₂ (b) y = 0.65H₂

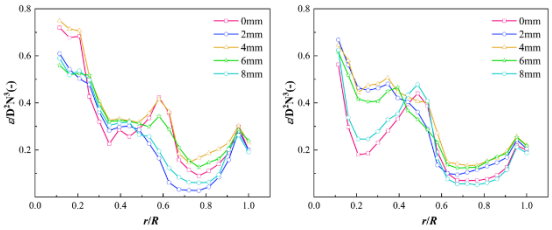

Figure 12. Effect of arc-chord distance on the dissipation rate of local radial turbulent kinetic energy (a) y = 0.25H₂ (b) y = 0.65H₂

5.4. The effect of blade angle

Figures 13 and 14 depict the profiles of dimensionless turbulent kinetic energy and turbulent energy dissipation rate, respectively, for varied blade angles. CBT accomplishes a judicious transition between axial and radial flows through blade angle adjustment. The turbulent kinetic energy and turbulent energy dissipation rate exhibit an initial rise in tandem with an increase in blade angle; however, they exhibit a marginal reduction when the blade angle surpasses a certain threshold. The most noteworthy escalation in both turbulent kinetic energy and turbulent energy dissipation rate is discerned at a blade angle of 50°.

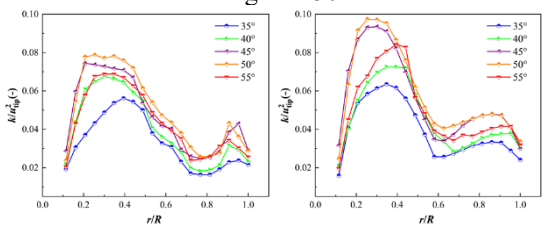

Figure 13. Effect of blade angle on the kinetic energy of local radial turbulence (a) y = 0.25H₂ (b) y = 0.65H₂

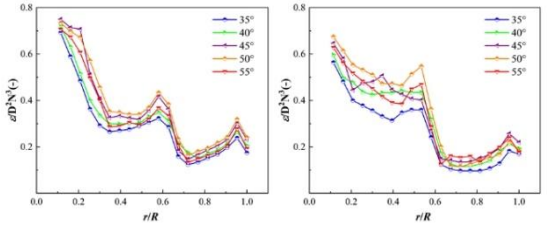

Figure 14. Effect of blade angle on the kinetic energy dissipation rate of local radial turbulence (a) y = 0.25H₂ (b) y = 0.65H₂

5.5. PIV experiments

A CBT with an arc chord distance of 4 mm and a blade angle of 50° was processed and analyzed for PIV experiments. The volume fraction distribution of solid phase particles in the stirred tank is shown in Figure 15, where it can be seen that the particle buildup at the bottom of the CBT is significantly lower than that of the PBT, and the upper clear zone is significantly reduced. Figure 16 shows the velocity distribution of the particles in the stirred tank. It can be seen that the degree of axial circulation of CBT particles is obviously increased, and the transient visible moving particles are obviously increased, which indicates that the suspension effect of particles in the stirring tank of CBT is obviously better than that of PBT, and proves that the analytical results are reliable.

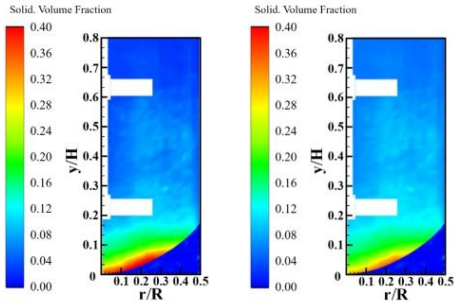

Figure 15. Volume fraction of solid particles measured by PIV (a) PBT (b) CBT

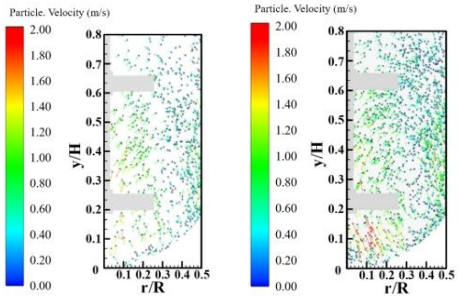

Figure 16. Particle velocity distribution measured by PIV experiment

6. CONCLUSION

In this paper, the MRGP approximation model and EFAST sensitivity analysis method are used to optimize the solid-liquid mixing performance of the double-impeller stirred tank under solid-liquid mixing conditions, and the optimization results are verified by PIV experiments. The main conclusions are as follows:

(1) The CBT impeller generates a high-speed jet during the rotation process, which effectively reduces the wake vortex scale and increases the turbulent kinetic energy and turbulent dissipation rate, thereby improving the solid-liquid suspension quality.

(2) The curved blade parameters significantly impact the solid-liquid mixing performance within stirred tanks. When the arc chord spacing is 4mm and the blade inclination angle is 50°, the mixing performance of the stirred tank can be significantly enhanced while reducing power usage.

(3) In this paper, the influence of arc blade parameters on mixing performance is systematically studied, which provides theoretical guidance for the design of non-standard curved blade turbines in similar stirred tanks.

ACKNOWLEDGEMENTS

This research is supported by the National Natural Science Foundation of China (Grant no. 51706203) and the Natural Science Foundation of Zhejiang Province exploration project (Y,LY20E090004). Thanks to ZJUT for providing computing resources and technical support, The authors also appreciateall other scholars' advice and assistance in improving this article.

REFERENCES

[1] Hu X, Ilgun AD, Passalacqua A, et al. CFD simulations of stirred-tank reactors for gas-liquid and gas-liquid-solid systems using OpenFOAM (R). International Journal of Chemical Reactor Engineering 2021; 19: 193-207. Article.

[2] Ramm P, Terboven C, Neitmann E, et al. Optimized production of biomethane as an energy vector from low-solids biomass using novel magnetic biofilm carriers. Applied Energy 2019; 251. Article.

[3] Fan L, Wang WJ, Yang C, et al. Numerical simulation of laminar flow field in a stirred tank. Chinese Journal of Chemical Engineering 2004; 12: 324-329. Article.

[4] Carletti C, Bikic S, Montante G, et al. Mass Transfer in Dilute Solid-Liquid Stirred Tanks. Industrial & Engineering Chemistry Research 2018; 57: 6505-6515. Article.

[5] Montante G and Magelli F. Modelling of solids distribution in stirred tanks: analysis of simulation strategies and comparison with experimental data. International Journal of Computational Fluid Dynamics 2005; 19: 253-262.

[6] Gu DY, Cheng C, Liu ZH, et al. Numerical simulation of solid-liquid mixing characteristics in a stirred tank with fractal impellers. Advanced Powder Technology 2019; 30: 2126-2138.

[7] Davoody M, Raman AAA, Ahmadi A, et al. Determination of Volumetric Mass Transfer Coefficient in Gas-Solid-Liquid Stirred Vessels Handling High Solids Concentrations: Experiment and Modeling. Iranian Journal of Chemistry & Chemical Engineering-International English Edition 2018; 37: 195-212.

[8] Kumaresan T and Joshi JB. Effect of impeller design on the flow pattern and mixing in stirred tanks. Chemical Engineering Journal 2006; 115: 173-193.

[9] Micheletti M, Nikiforaki L, Lee KC, et al. Particle concentration and mixing characteristics of moderate-to-dense solid-liquid suspensions. Industrial & Engineering Chemistry Research 2003; 42: 6236-6249.

[10] Guha D, Ramachandran PA, Dudukovic MP, et al. Evaluation of large Eddy simulation and Euler-Euler CFD models for solids flow dynamics in a stirred tank reactor. Aiche Journal 2008; 54: 766-778.

[11] Montante G, Paglianti A and Magelli F. Analysis of dilute solid-liquid suspensions in turbulent stirred tanks. CHEMICAL ENGINEERING RESEARCH & DESIGN 2012; 90: 1448-1456.

[12] Wu B. CFD PREDICTION OF MIXING TIME IN ANAEROBIC DIGESTERS. Transactions of the Asabe 2010; 53: 553-563.

[13] Wu BX. COMPUTATIONAL FLUID DYNAMICS STUDY OF LARGE-SCALE MIXING SYSTEMS WITH SIDE-ENTERING IMPELLERS. Engineering Applications of Computational Fluid Mechanics 2012; 6: 123-133.

[14] Liu L, Chen ZB, Yan HJ, et al. Numerical simulation of gas-liquid heat and mass transfer in pressurized leaching stirred tanks[J]. Transactions of Nonferrous Metals Society of China, 2022, 32(10): 3111-3122.

[15] Wang SY, Jiang XX, Wang RC, et al. Numerical simulation of flow behavior of particles in a liquid-solid stirred vessel with baffles. Advanced Powder Technology 2017; 28: 1611-1624.

[16] Liu FC, Wei PF, Tang CH, et al. Global sensitivity analysis for multivariate outputs based on multiple response Gaussian process model. Reliability Engineering & System Safety 2019; 189: 287-298.

[17] Kumaresan T, Nere NK and Joshi JB. Effect of internals on the flow pattern and mixing in stirred tanks. Industrial & Engineering Chemistry Research 2005; 44: 9951-9961.